



Absence of hydrogen insertion into highly crystalline superconducting infinite layer nickelatesM. Gonzalez ^{*}*Stanford Institute for Materials and Energy Sciences, SLAC National Accelerator Laboratory, Menlo Park, California 94025, USA
and Department of Materials Science and Engineering, Stanford University, Stanford, California 94305, USA*

A. Ievlev

*Center for Nanophase Material Science, Oak Ridge National Laboratory, Oak Ridge, Tennessee 37830, USA*K. Lee *Stanford Institute for Materials and Energy Sciences, SLAC National Accelerator Laboratory, Menlo Park, California 94025, USA
and Department of Physics, Stanford University, Stanford, California 94305, USA*W. Kim, Y. Yu , J. Fowlie,[†] and H. Y. Hwang *Stanford Institute for Materials and Energy Sciences, SLAC National Accelerator Laboratory, Menlo Park, California 94025, USA
and Department of Applied Physics, Stanford University, Stanford, California 94305, USA*

(Received 27 June 2024; accepted 30 July 2024; published 12 August 2024)

The discovery of superconductivity in the infinite layer nickelates introduced a materials system analogous to the cuprates for the study of unconventional superconductivity. The synthesis of infinite layer nickelates, (RNiO_2) , $\text{R} = \text{lanthanide}$) often uses calcium hydride (CaH_2) to facilitate the deintercalation of apical site oxygen atoms from a precursor perovskite (RNiO_3) phase via topotactic reduction. However, it remains uncertain whether the use of CaH_2 results in the insertion of hydrogen into the infinite layer structure, and if it does, what the implications are for superconductivity. To quantify the hydrogen composition of highly crystalline infinite layer nickelates, we synthesized $\text{Nd}_{1-x}\text{Sr}_x\text{NiO}_2$ thin films on LSAT substrates and conducted time-of-flight secondary ion mass spectroscopy measurements to generate hydrogen depth profiles. We compare the hydrogen density of nickelates prepared with and without a SrTiO_3 capping layer. Additionally, we measure the hydrogen content in nickelate samples at various doping levels spanning the superconducting phase space, including the underdoped, optimally doped, and overdoped regime. We report no significant increase in hydrogen density between the perovskite and infinite layer phases in any of the measured samples. Furthermore, we put an upperbound on the hydrogen concentration of our nickelate samples to $\text{Nd}_{1-x}\text{Sr}_x\text{NiO}_2\text{H}_{0.05}$. Our results imply that hydrogen is not responsible for the emergence of superconductivity in the infinite layer nickelates.

DOI: [10.1103/PhysRevMaterials.8.084804](https://doi.org/10.1103/PhysRevMaterials.8.084804)**I. INTRODUCTION**

Infinite layer nickelates have emerged as promising candidates for the study of unconventional superconductivity because of their electronic and structural similarities with the cuprates [1,2]. Nickel-based superconductivity was first realized in strontium-doped neodymium nickel oxide $(\text{Nd, Sr})\text{NiO}_2$ [3], sparking a plethora of investigations into Ni-based compounds [4]. Since its initial discovery, a rich phase diagram has been uncovered including a robust superconducting dome [5–9], magnetic fluctuations [10], and other ordered phases [11–14].

Historically, experimental studies into the nickelates have been limited because the poor thermodynamic stability of the system constrains superconductivity to nanometer-scale epitaxial thin films, which has introduced challenges to

reproducibility [15,16]. Synthesis of this material system is a two-step process: first involving the growth of the precursor perovskite phase; followed by the removal of apical site oxygen atoms via topotactic reduction. Fortunately, recent work has shown tremendous progress toward the synthesis of high quality infinite layer nickelates. For instance, the use of a SrTiO_3 (STO) capping layer protects thin films from degradation via reoxidation and prevents the formation of impurity phases [17]. Furthermore, moving perovskite phase growth onto LSAT substrates has shown a reduced defect density of the resultant infinite layer structure [6].

Topotactic reactions have emerged as a powerful technique for the synthesis of metastable oxide phases by selectively removing (or inserting) mobile species while preserving the host lattice [18]. These structural transformations enable host atoms to adopt unusual oxidation states and coordination environments [19]. Hence, topochemistry provides an avenue to manipulate the electronic properties of oxide systems, including the low-temperature fluorination of alkaline-earth cuprates to induce superconductivity [20]. Novel thin film

^{*}Contact author: martin99@stanford.edu[†]Contact author: jfowlie@stanford.edu

materials produced via topotactic transitions include CaCoO_2 [21], SrFeO_2 [22], and SrVO_2H [23]. In the case of nickelate superconductors, topotactic reduction is pivotal in the stabilization of an unusual monovalent oxidation state Ni^+ , assuming a d^9 electronic configuration. The reduction of nickelates has been achieved using a variety of means; including reaction with gaseous H_2 environment [24], reaction with metal hydrides [24–27], and *in situ* metallic reduction [28].

However, it remains uncertain whether topotactic reduction results in the insertion of hydrogen into superconducting nickelates. The use of gaseous hydrogen or metallic hydrides for reduction introduces the possibility of hydrogen incorporation into either interstitial sites or apical oxygen sites. It has become established that reduction of perovskite nickelates into the infinite layer structure may occur via a variety of intermediary structural phases consisting of ordered oxygen vacancies [12,24,27]. Incomplete reduction processes may result in mixed-phase nickelate samples, whose secondary phases may host hydrogen. Additionally, infinite layer nickelates prepared without an STO capping layer have revealed impurity phases, including a hydrogen-rich fluorite structure [29], sitting above the infinite layer region [17]. The secondary phases that arise from suboptimal nickelate synthesis present opportunities for hydrogen incorporation during topotactic reduction.

Multiple computational and experimental studies paint a conflicting view on the presence and role of topotactic hydrogen for superconductivity in the infinite layer nickelates. Density functional theory calculations have suggested that oxyhydride formation is energetically favorable only at low hole-doping levels [30,31]. Among experimental studies, topotactic hydrogen was detected in bulk powdered samples of LaNiO_2 , but was deduced to be confined to grain boundaries or secondary-phase precipitates [32].

A growing collection of hydrogen depth profile experiments using ToF-SIMS further complicates our understanding of the effect hydrogen may have on the nickelates. For instance, Onozuka *et al.* (2016) used ToF-SIMS depth profiling to show substantial hydrogen incorporation into an impurity fluorite phase sitting above the infinite layer structure [29]. Subsequently, Ding *et al.* (2023) observed orders-of-magnitude increase in hydrogen upon reduction of perovskite nickelates, and argued that hydrogen plays an important role for the emergence of superconductivity [33]. However, recent experiments have found negligible hydrogen content in a variety of nickelate samples [34,35]. The contradictory conclusions drawn about the presence of topotactic hydrogen prompts two important questions: whether hydrogen insertion is inevitably tied to nickelate synthesis, and whether the presence of hydrogen is important for the emergence of superconductivity.

In this work, we seek to resolve the debate on whether infinite layer nickelates synthesized using calcium hydride (CaH_2) results in hydrogen intercalation. Our work leverages advances in nickelate synthesis to determine whether hydrogen is present in the highest quality nickelate samples. We used time-of-flight secondary ion mass spectroscopy (ToF-SIMS) to generate hydrogen depth profiles of $(\text{Nd}, \text{Sr})\text{NiO}_2$ (NSNO) thin films after reduction. We focus specifically on comparing the hydrogen content in superconducting

nickelates prepared with and without an STO capping layer. We seek to understand whether the reduced crystallinity resulting from the absence of a capping layer is responsible for the presence of topotactic hydrogen. In addition, we explore the hydrogen content of a nickelate doping series representative of the underdoped, optimallydoped, and overdoped regimes of the phase diagram. We hope to clarify whether there is a dependence between doping level and the hydrogen density of the samples. Overall, we report no significant increase in hydrogen density in any NSNO thin film with a maximum hydrogen composition given by $\text{Nd}_{1-x}\text{Sr}_x\text{NiO}_2\text{H}_{0.05}$. Hence, we conclude that hydrogen is not responsible for the emergence of superconductivity in the infinite layer nickelates.

II. EXPERIMENTAL DETAILS

Precursor perovskite thin films were deposited onto $(\text{La}_{0.3}\text{Sr}_{0.7})(\text{Al}_{0.65}\text{Ta}_{0.35})\text{O}_3$ (001) (LSAT, Shinkosha Co) substrates by pulsed laser deposition using the optimal conditions reported in Lee *et al.* (2023) [6]. Note that LSAT is inert against CaH_2 reduction, and thus can serve as the background hydrogen density [36]. The perovskite films were subsequently wrapped in aluminum foil and reacted with 0.1 g CaH_2 powder within a vacuum-sealed Pyrex glass tube (<5 mtorr). The tube was heated to a temperature of 320 °C and annealed for approximately three hours.

The crystalline quality of the perovskite and infinite layer nickelate phases were determined using x-ray diffraction (XRD) $2\theta - \omega$ symmetric scans. Figure 1(a) shows the XRD diffraction patterns for all samples investigated for hydrogen incorporation. Representative samples of interest include the optimally doped (17.5% Sr doped) superconducting thin films, one prepared with an STO capping layer (in orange) and one prepared without a capping layer (in red). Reports have indicated that the presence of an STO capping layer (or lack thereof) may influence the properties of the infinite layer nickelates [37], which may affect the presence of hydrogen in the system. Furthermore, STEM images of uncapped infinite layer nickelates have revealed impurity secondary phases occupying the surface layers of the nickelate [17]. Here, we demonstrate the effect of an STO capping layer on the crystalline quality and superconducting properties of optimally doped infinite layer nickelates.

Symmetric scan fitting of the diffraction patterns is achieved using a MATLAB XRD simulation [38]. The diffraction pattern for the capped sample shows a thin film thickness of 13 unit cells (~ 5 nm) with an extracted c -lattice constant $c = 3.74$ Å. Topotactic reduction into the infinite layer phase is demonstrated by a rightward shift of the thin film peak position, indicating a contraction of the c -lattice constant towards $c = 3.33$ Å. Additionally, the XRD diffraction patterns shows a complete conversion into the infinite layer phase, with no indication of any secondary phases. Therefore, we confirm a complete topotactic reduction of the precursor perovskite into the reduced infinite layer phase with thickness of ~ 4.4 nm (13 u.c). The temperature-dependent resistivity, as shown in Figs. 1(b) and 1(c), demonstrates a superconducting transition at $T_{c,\text{onset}} = 18$ K and zero-resistance state achieved at $T_{c,0} = 12.5$ K. At temperatures above the superconducting transition

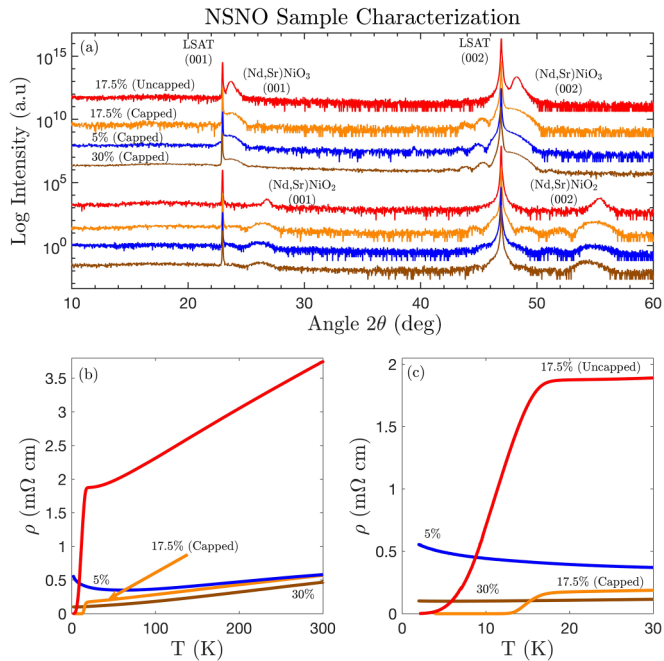


FIG. 1. (a) XRD $2\theta - \omega$ symmetric scans of perovskite nickelate thin films (upper four diffraction patterns) and their reduced infinite layer form (lower four diffraction patterns). From top to bottom, these samples include an uncapped 17.5% Sr-doped (~ 15 nm as-grown), capped 17.5% Sr-doped (~ 5 nm as-grown), capped 5% Sr-doped (~ 5 nm as-grown) and capped 30% Sr-doped (~ 5 nm as-grown) thin films grown on LSAT (001) substrate. (b) Temperature-dependent resistivity curves for each infinite layer nickelate along with (c) a close up view at low temperatures up to 30 K.

the resistivity ranges between 0.20–0.55 m Ω cm and scales linearly with temperature, consistent with previous reports [6].

We prepared an uncapped superconducting NSNO film to probe the hydrogen content of samples with reduced crystallinity. The XRD $2\theta - \omega$ symmetric scan shows a precursor perovskite thin film with a thickness of 39 unit cells (~ 15 nm) and an extracted c -lattice constant $c = 3.77$ Å. Note that the film was intentionally grown to be approximately three times thicker than the capped nickelate, making the sample more prone to surface decomposition [17,29]. We see the topotactic reduction to the infinite layer phase with an extracted c -lattice constant of $c = 3.32$ Å. However, this sample achieves an infinite layer phase conversion rate of approximately 87%, corresponding to about 1.8 nm of an unidentified structural phase, which may indicate some level of degradation [17]. The temperature dependent resistivity features a superconducting transition with $T_{c,\text{onset}} = 17$ K and a zero-resistance state at $T_{c,0} < 2$ K. In comparison to our capped sample, we see a broader superconducting transition with a lower zero-resistance $T_{c,0}$. Furthermore above the superconducting transition, resistivity ranges between 2–4 m Ω cm, an order of magnitude larger than the previously analyzed sample. The electrical transport properties show that the uncapped sample is quantitatively worse than our originally measured capped sample.

We also completed characterization measurements for nickelate samples at different doping levels. Figure 1 shows the full characterization data for the NSNO doping series which, in addition to the aforementioned optimally doped sample, includes an underdoped 5% Sr doped (blue), and an overdoped 30% Sr doped (brown) thin film, both prepared with an STO cap. These samples were synthesized from 5 nm as-grown perovskite phase nickelates with a 1.5 nm STO capping layer. Figure 1(a) shows the XRD diffraction patterns for each of the samples in the doping series. The XRD data all demonstrate robust high intensity precursor perovskite peaks indicative of high quality sample preparation. Each sample also exhibits a successful topotactic reduction with an infinite layer conversion rate $>90\%$ for all samples. The c axis lattice constants for the capped infinite layer samples in the underdoped, optimally doped, and overdoped regimes are 3.33 Å, 3.33 Å, and 3.36 Å, respectively. The temperature-dependent resistivity curves, shown in Figs. 1(b) and 1(c) also indicate high quality sample preparation with resistivities on the order of 0.1–0.6 m Ω cm. The low-temperature behavior is dependent on the doping level. The underdoped sample is characterized by an insulating upturn, the optimally doped sample shows a superconducting transition, and the overdoped sample remains metallic at low temperatures. The transport properties of each of these samples is consistent with their respective doping levels, as reported by previous literature [6].

III. HYDROGEN QUANTIFICATION

Hydrogen is an element that is not easily detected by most elemental analysis techniques. Therefore, we rely on ToF-SIMS which offers high elemental sensitivity, depth resolution, and mass resolution [39,40]. During a depth profile measurement, a focused stream of energetic ions, known as the primary ion beam, bombards the surface of the sample. The incident primary beam deposits energy onto the surface layers causing the ejection of constituent particles away from the sample surface, forming the secondary ion beam. The secondary ions are collected and pass through a mass spectrometer, which is subsequently analyzed to form a composition depth profile [41]. We used the ToF-SIMS instrumentation available at ORNL Center for Nanophase Materials Science (TOF.SIMS.5 NSC). Our measurements employed a dual-beam system which uses a sputtering beam dedicated to removing material from the sample surface, and a separate analysis beam responsible for producing secondary ions. The use of a dual-beam system allows for finer control of experimental parameters that are better optimized for thin film depth profile measurements [41]. We used a 0.5 keV Cs^+ sputtering beam and a 30 keV Bi^+ analysis beam which are suitable beam conditions for depth profiling of thin films on hard substrates [42]. Measurements were carried out in a noninterlaced mode, where each analysis scan by the Bi^+ primary ion source was followed by sputtering with the Cs^+ source for 2 s. The TOF analyzer was operated in positive-ion mode, hence we collected data on H^+ and other positively charged species. Depth calibration was calculated using the sample thickness extracted from XRD measurements under the assumption of homogeneous sputter rates.

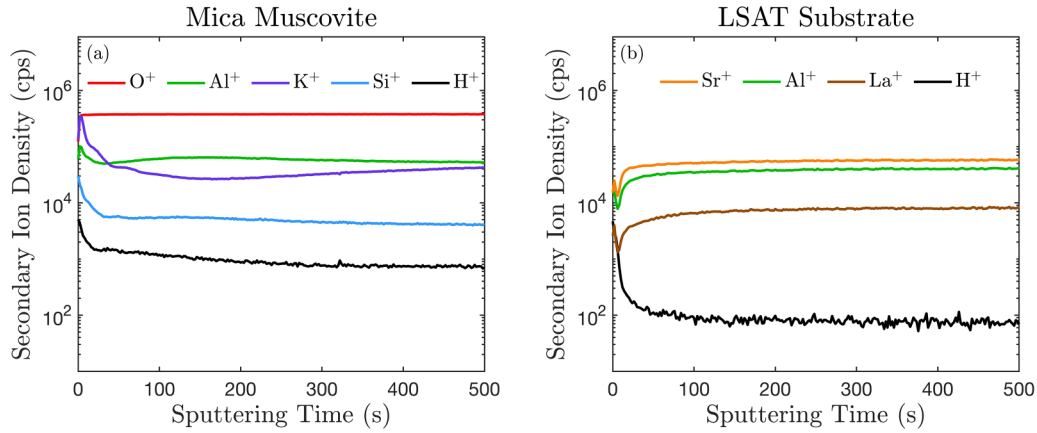


FIG. 2. (a) ToF-SIMS depth profile for mica muscovite standard reference, with oxygen, aluminum, potassium, silicon, and hydrogen signals represented. Away from the surface, the hydrogen signal is on the order of 10^3 cps. (b) ToF-SIMS depth profile for bare LSAT substrate with strontium, aluminum, lanthanum, and hydrogen signals represented. The saturated hydrogen secondary ion signal $\sim 10^2$ was used to scale subsequent ion densities into hydrogen concentrations.

Hydrogen is an extremely abundant chemical species present in a variety of solid-state materials. Depth profiling experiments have measured a baseline hydrogen concentration on the order of 10^{19} – 10^{20} atoms/cm³ in silicon [43,44], glass [45], and semiconductor oxides [46,47]. Similar background levels have been measured in substrates used for perovskite thin films [48,49]. The accepted detection limit for time-of-flight SIMS depth profiling is on the order of a few 10^{19} atoms/cm³, sensitive enough for our probe into potential hydrogen insertion into the nickelates [50].

However, ToF-SIMS is a qualitative analysis technique that offers information about the relative abundance of constituent elements. Therefore, hydrogen quantification requires a comparison with a reference material of known hydrogen content. We used mica muscovite, $\text{KAl}_2[\text{AlSi}_3\text{O}_{10}](\text{OH})_2$, as a reliable solid state reference with known hydrogen density. Mica muscovite has previously been used as a standard reference for hydrogen quantification in the infinite layer nickelates, allowing for direct comparison of hydrogen content with our experimental results [33]. Despite the imperfect chemical matrix matching between mica muscovite and nickel oxides, mica is known to be a suitable chemical standard given its strongly bound hydroxide ions, high thermal stability, and limited concentration variation [51]. Furthermore, mica is known to be a reference of a well-defined layered structure for analysis of geological specimens [52]. Therefore, we are able to provide an estimated upper limit in the hydrogen content of the infinite layer nickelates.

Figure 2(a) shows the depth profile for mica muscovite, which includes data for oxygen, aluminum, potassium, silicon, and hydrogen chemical species. The depth profile shows a bulk hydrogen intensity on the order of 10^3 cps. Note that mica muscovite has a known hydrogen density of $n_{\text{H, Mica}} = 8.3 \times 10^{21}$ cm⁻³. In Fig. 2(b) we show the depth profile for a bare LSAT substrate with strontium, aluminum, lanthanum, and hydrogen chemical species represented. The hydrogen secondary ion density in LSAT is on the order of 10^2 cps. Hence, the substrate hydrogen density was calculated by scaling the hydrogen signal between the mica standard reference

and the bare LSAT substrate. The background LSAT hydrogen density was calculated to be approximately $n_{\text{H, LSAT}} = 7.0 \times 10^{20}$ cm⁻³, comparable with the substrate density calculated in previous ToF-SIMS studies [29,48].

IV. RESULTS AND DISCUSSION

Proper interpretation of ToF-SIMS depth profiles requires an understanding of how the sputtering process may alter secondary ion yield. For instance, beam-induced surface roughening occurs when the sputtering ion beam induces changes to the sample's surface topography [42,53]. Surface roughening usually manifests itself in degraded surface resolution and enhanced (or depressed) signal intensity at the onset of measurement. These effects can be minimized by using a small beam size and reducing the sample's initial surface roughness. Atomic force microscopy characterization of our nickelate samples confirms a mostly flat surface with a root-mean-squared roughness on the order of angstroms. Therefore, we can anticipate that surface roughening will play a small role in the interpretation of our depth profiles.

ToF-SIMS is also highly sensitive to surface contamination, especially from salt ions and organic matter. Of particular importance, hydrocarbon contamination will produce an enhanced hydrogen signal at the surface of the depth profile. While great care was taken to minimize surface contamination, it is difficult to prevent the deposition of a surface hydrocarbon layer that is almost instantaneously formed upon removal from a high vacuum chamber [42]. Previous depth profile studies of oxide thin films have observed this effect, including in the infinite layer cobaltates [21] and in the infinite layer nickelates [29,33–35]. Therefore, we can expect an enhanced surface hydrogen signal that we attribute to contamination. Finally, the influence of matrix effects on secondary ion generation can impact the shape and magnitude of depth profile signals. These effects are evident at the interface of distinct material layers where the change in ionization efficiency may manifest in the appearance of nonsharp interfaces [54].

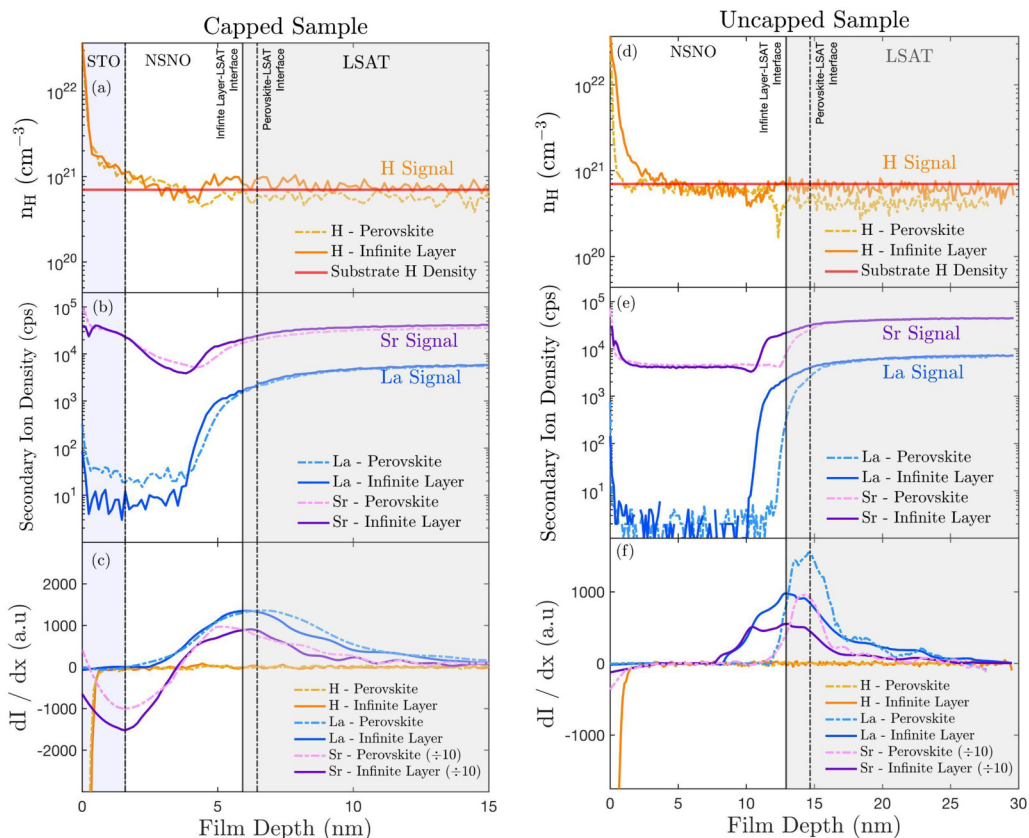


FIG. 3. ToF-SIMS composition depth profiles for the (a)–(c) optimally doped NSNO thin film nickelate prepared with an STO cap and (d)–(f) an optimally doped, uncapped NSNO thin film. (a), (d) The measured hydrogen density is plotted as a function of film depth. Solid (dash dotted) lines denote the hydrogen density of the infinite layer (perovskite) phases. The red horizontal line shows the hydrogen density measured in the bare LSAT substrate. The region shaded in gray signifies the LSAT substrate whereas light blue signifies the STO capping layer in the capped sample. (b), (e) Secondary ion density for Sr and La chemical species as a function of film depth aid in identification of substrate–film and STO cap–film interfaces. (c), (f) Derivative of the infinite layer signal for each chemical species as a function of film depth. The maximal La signal derivative was used to identify the film–substrate interface, while the minimal Sr signal derivative aids in identifying the STO cap, thin film interface.

Figure 3(a) shows the hydrogen depth profile for the capped, optimally doped NSNO sample in both its perovskite (dashed dotted lines) and infinite layer phase (solid lines). The hydrogen secondary-ion density is scaled into a particle density using the mica standard reference. The STO cap is shaded in light blue and is featured in the first 1.5 nm of the depth profile, whereas the LSAT substrate is shaded in light gray and extends beyond 6.5 nm into the depth profile. A solid vertical line marks the interface between the infinite layer thin film and the substrate; whereas a dashdotted vertical line marks the substrate–thin film interface for the perovskite phase prior to topotactic reduction. In between the shaded regions, we show the hydrogen density for the NSNO thin film. Additionally, a horizontal red line shows the background hydrogen density from the LSAT substrate. The strontium and lanthanum secondary-ion densities are plotted in Fig. 3(b), where the shape and magnitude of their depth profile are reflective of the heterostructure. These signals facilitate in the identification of the STO cap–thin film interface and the thin film–substrate interface. A more quantitative identification is achieved by plotting the derivative of each chemical species’ signal with respect to sample depth, as is shown in Fig. 3(c). We rely on the derivative of the Sr and La signal intensities to

determine sample interfaces taking the minimum Sr derivative as the STO–thin film interface, and the peak La derivative as the thin film–substrate interface.

In the case of the capped superconducting NSNO, the hydrogen depth profile reveals negligible difference in hydrogen concentration between the perovskite and infinite layer phases. Furthermore, the hydrogen content is on the same order-of-magnitude with respect to the background substrate level. Within our experimental resolution, there is no depth dependence of the hydrogen content as indicated by $dI_H/dx \approx 0$. Within the thin film region, the hydrogen density rarely exceeds $1.0 \times 10^{21} \text{ cm}^{-3}$ in either structural phase, corresponding to an upper-bound in hydrogen composition given by $\text{Nd}_{0.825}\text{Sr}_{0.175}\text{NiO}_2\text{H}_{0.05}$. This level of hydrogen content is an order of magnitude lower than estimated by previous experimental reports which claim hydrogen content as high as 45% [32,33]–70% [29]. These results show that it is possible to synthesize the infinite layer structure through the use of CaH_2 without introducing significant levels of hydrogen. Furthermore, the nickelate achieves a robust superconducting state, establishing that hydrogen is not necessary for the emergence of superconductivity. This conclusion is corroborated by reports of superconducting nickelates synthesized

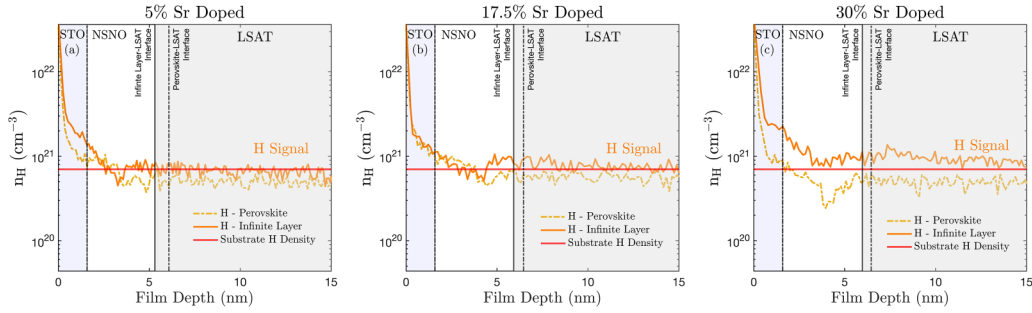


FIG. 4. (a) Hydrogen depth profile for capped 5% (underdoped) NSNO sample in both perovskite and infinite layer phases. (b) Analogous hydrogen depth profiles for 17.5% (optimally doped), (c) and 30% (overdoped) NSNO samples. The sample interfaces shown here were determined quantitatively using the derivative of Sr and La chemical signals with respect to film depth.

using *in situ* metallic reduction, which does not involve a hydride compound [28]. Negligible hydrogen insertion is similarly reported by Balakrishnan *et al.* (2024) and Zeng *et al.* (2024).

We also acquired a hydrogen depth profile on an uncapped sample with a lower infinite layer conversion ratio, wider superconducting transition, and lower $T_{c,0}$ as discussed in Sec. II. Figure 3(d) shows the hydrogen depth profile of the uncapped nickelate in both the perovskite and infinite layer phases. As before, the NSNO hydrogen concentration for both structural phases remains unchanged with respect to the substrate background level. In fact, the hydrogen density for the NSNO film remains consistently under $n_H < 8 \times 10^{20} \text{ cm}^{-3}$, corresponding to a maximum hydrogen composition of $\text{Nd}_{0.825}\text{Sr}_{0.175}\text{NiO}_2\text{H}_{0.04}$. Unlike previous reports, we do not see orders of magnitude difference in the hydrogen signal intensity between the perovskite and infinite layer phases [29,33]. Figure 3(e) shows the lanthanum and strontium signals. The differential signal intensities for all samples are also shown in Fig. 3(f), where the peak value for the La derivative was used for substrate interface identification. The observed rise in hydrogen signal within the first 2.5 nm, which is reflected by its large signal derivative, can mostly be attributed to surface contamination and decomposition [29]. Despite our sample exhibiting degraded superconducting properties due to the lack of a SrTiO_3 capping layer, there is no evidence for hydrogen incorporation in the thin film.

Finally, we acquired hydrogen depth profiles for the NSNO doping series, including the under-doped, optimally-doped, and over-doped regime; as seen in Fig. 4. Like before, each depth profile shows the hydrogen density of the perovskite (dash-dotted) and infinite layer (solid) structures; with the red line indicating the background hydrogen level determined by the bare LSAT substrate. The STO cap and LSAT substrate regions of the depth profile are similarly labeled as before. Each of these samples continue to show no order-of-magnitude increase in hydrogen content upon reduction into the infinite layer phase. However, there appears to be a slight increase of hydrogen content at higher doping levels. We attribute this to an expanded *c*-lattice constant and reduced crystallinity due to the challenge of stabilizing the high Ni oxidation state in the perovskite precursor. This observation runs contrary to DFT calculations which suggest greater hydrogen favorability at low doping. However, even in the overdoped sample, we place an upper bound on hydrogen content at 5% ($\sim 10^{21} \text{ cm}^{-3}$).

These samples demonstrate that significant amounts of hydrogen do not enter the infinite layer structure, regardless of doping level. This finding furthers the argument that hydrogen does not contribute to the observed superconducting properties of the infinite layer nickelates.

V. CONCLUSION

In this report we investigated the possibility of incorporating hydrogen into infinite layer nickelates via CaH_2 induced topotactic reduction. Our study takes advantage of improved synthesis conditions that produce highly crystalline nickelate thin films. Using ToF-SIMS depth profiling measurements, we found that hydrogen was not intercalated into our infinite layer nickelates during topotactic reduction, even in the absence of an STO cap. The emergence of superconductivity in our samples demonstrates that topotactic hydrogen is not required for unconventional superconductivity in the infinite layer nickelates. Furthermore, we found that hydrogen was not found to enter the infinite layer nickelates at various doping levels in the superconducting state, as well as in the normal state. From our observations in both XRD and transport, we believe that the lack of topotactic hydrogen is a result of the highly crystalline quality of our samples. However, we cannot exclude the possibility that other experimental variables such as substrate choice, thin film thickness, or rare-earth cation could result in hydrogen insertion. Follow-up work is needed to elucidate the mechanism from which hydrogen enters nickelate thin films and what effects it has on its electronic behavior. These suggested studies would improve our understanding of the synthesis of infinite layer nickelates and deepen our knowledge of the topotactic reduction process.

ACKNOWLEDGMENTS

This work was supported by the U.S. Department of Energy, Office of Basic Energy Sciences, Division of Materials Sciences and Engineering (Contract No. DE-AC02-76SF00515) and the Gordon and Betty Moore Foundation's Emergent Phenomena in Quantum Systems Initiative (Grant No. GBMF9072, synthesis equipment). Part of this work was performed at the Stanford Nano Shared Facilities (SNSF), supported by the National Science Foundation under Award No. ECCS-2026822. Part of this research was conducted at the Center for Nanophase Materials Sciences, which is a DOE

Office of Science User Facility and using instrumentation within ORNL's Materials Characterization Core provided by

UT-Battelle, LLC under Contract No. DE-AC05-00OR22725 with the U.S. Department of Energy.

- [1] K.-W. Lee and W. E. Pickett, Infinite-layer LaNiO_2 : Ni^{1+} is not Cu^{2+} , *Phys. Rev. B* **70**, 165109 (2004).
- [2] A. S. Botana and M. R. Norman, Similarities and differences between LaNiO_2 and CaCuO_2 and implications for superconductivity, *Phys. Rev. X* **10**, 011024 (2020).
- [3] D. Li, K. Lee, B. Y. Wang, M. Osada, S. Crossley, H. R. Lee, Y. Cui, Y. Hikita, and H. Y. Hwang, Superconductivity in an infinite-layer nickelate, *Nature (London)* **572**, 624 (2019).
- [4] X. Zhou, P. Qin, Z. Feng, H. Yan, X. Wang, H. Chen, Z. Meng, and Z. Liu, Experimental progress on the emergent infinite-layer Ni-based superconductors, *Mater. Today* **55**, 170 (2022).
- [5] D. Li, B. Y. Wang, K. Lee, S. P. Harvey, M. Osada, B. H. Goodge, L. F. Kourkoutis, and H. Y. Hwang, Superconducting dome in $\text{Nd}_{1-x}\text{Sr}_x\text{NiO}_2$ infinite layer films, *Phys. Rev. Lett.* **125**, 027001 (2020).
- [6] K. Lee, B. Y. Wang, M. Osada, B. H. Goodge, T. C. Wang, Y. Lee, S. Harvey, W. J. Kim, Y. Yu, C. Murthy, S. Raghu, L. F. Kourkoutis, and H. Y. Hwang, Linear-in-temperature resistivity for optimally superconducting (Nd, Sr) NiO_2 , *Nature (London)* **619**, 288 (2023).
- [7] M. Osada, B. Y. Wang, B. H. Goodge, S. P. Harvey, K. Lee, D. Li, L. F. Kourkoutis, and H. Y. Hwang, Nickelate superconductivity without rare-earth magnetism: (La, Sr) NiO_2 , *Adv. Mater.* **33**, 2104083 (2021).
- [8] S. Zeng, C. S. Tang, X. Yin, C. Li, M. Li, Z. Huang, J. Hu, W. Liu, G. J. Omar, and H. Jani, Phase diagram and superconducting dome of infinite-layer $\text{Nd}_{1-x}\text{Sr}_x\text{NiO}_2$ thin films, *Phys. Rev. Lett.* **125**, 147003 (2020).
- [9] S. Zeng, C. Li, L. E. Chow, Y. Cao, Z. Zhang, C. S. Tang, X. Yin, Z. S. Lim, J. Hu, and P. Yang, Superconductivity in infinite-layer nickelate $\text{La}_{1-x}\text{Ca}_x\text{NiO}_2$ thin films, *Sci. Adv.* **8**, eabl9927 (2022).
- [10] J. Fowlie, M. Hadjimichael, M. M. Martins, D. Li, M. Osada, B. Y. Wang, K. Lee, Y. Lee, Z. Salman, and T. Prokscha, Intrinsic magnetism in superconducting infinite-layer nickelates, *Nat. Phys.* **18**, 1043 (2022).
- [11] M. Rossi, M. Osada, J. Choi, S. Agrestini, D. Jost, Y. Lee, H. Lu, B. Y. Wang, K. Lee, A. Nag, Y.-D. Chuang, C.-T. Kuo, S.-J. Lee, B. Moritz, T. P. Devereaux, Z.-X. Shen, J.-S. Lee, K.-J. Zhou, H. Y. Hwang, and W.-S. Lee, A broken translational symmetry state in an infinite-layer nickelate, *Nat. Phys.* **18**, 869 (2022).
- [12] C. T. Parzyck, N. K. Gupta, Y. Wu, V. Anil, L. Bhatt, M. Bouliane, R. Gong, B. Gregory, A. Luo, R. Sutarto *et al.*, Absence of $3a_0$ charge density wave order in the infinite-layer nickelate NdNiO_2 , *Nat. Mater.* **23**, 486 (2024).
- [13] G. Krieger, L. Martinelli, S. Zeng, L. E. Chow, K. Kummer, R. Arpaia, M. Moretti Sala, N. B. Brookes, A. Ariando, N. Viart, M. Salluzzo, G. Ghiringhelli, and D. Preziosi, Charge and spin order dichotomy in NdNiO_2 driven by the capping layer, *Phys. Rev. Lett.* **129**, 027002 (2022).
- [14] C. C. Tam, J. Choi, X. Ding, S. Agrestini, A. Nag, M. Wu, B. Huang, H. Luo, P. Gao, and M. García-Fernández, Charge density waves in infinite-layer NdNiO_2 nickelates, *Nat. Mater.* **21**, 1116 (2022).
- [15] M. Zinkevich, N. Solak, H. Nitsche, M. Ahrens, and F. Aldinger, Stability and thermodynamic functions of lanthanum nickelates, *J. Alloys Compd.* **438**, 92 (2007).
- [16] D. Preziosi, A. Sander, A. Barthélémy, and M. Bibes, Reproducibility and off-stoichiometry issues in nickelate thin films grown by pulsed laser deposition, *AIP Adv.* **7**, 015210 (2017).
- [17] K. Lee, B. H. Goodge, D. Li, M. Osada, B. Y. Wang, Y. Cui, L. F. Kourkoutis, and H. Y. Hwang, Aspects of the synthesis of thin film superconducting infinite-layer nickelates, *APL Mater.* **8**, 041107 (2020).
- [18] M. Hayward, Topochemical reactions of layered transition-metal oxides, *Semicond. Sci. Technol.* **29**, 064010 (2014).
- [19] Z. Meng, H. Yan, P. Qin, X. Zhou, X. Wang, H. Chen, L. Liu, and Z. Liu, Topotactic transition: A promising opportunity for creating new oxides, *Adv. Funct. Mater.* **33**, 2305225 (2023).
- [20] M. Francesconi, P. Slater, J. Hodges, C. Greaves, P. Edwards, M. Al-Mamouri, and M. Slaski, Superconducting $\text{Sr}_{2-x}\text{A}_x\text{CuO}_2\text{F}_{2+\delta}$ ($\text{A} = \text{Ca}, \text{Ba}$): Synthetic pathways and associated structural rearrangements, *J. Solid State Chem.* **135**, 17 (1998).
- [21] W. J. Kim, M. A. Smeaton, C. Jia, B. H. Goodge, B.-G. Cho, K. Lee, M. Osada, D. Jost, A. V. Ievlev, B. Moritz, L. F. Kourkoutis, T. P. Devereaux, and H. Y. Hwang, Geometric frustration of Jahn–Teller order in the infinite-layer lattice, *Nature (London)* **615**, 237 (2023).
- [22] Y. Tsujimoto, C. Tassel, N. Hayashi, T. Watanabe, H. Kageyama, K. Yoshimura, M. Takano, M. Ceretti, C. Ritter, and W. Paulus, Infinite-layer iron oxide with a square-planar coordination, *Nature (London)* **450**, 1062 (2007).
- [23] T. Katayama, A. Chikamatsu, K. Yamada, K. Shigematsu, T. Onozuka, M. Minohara, H. Kumigashira, E. Ikenaga, and T. Hasegawa, Epitaxial growth and electronic structure of oxyhydride SrVO_2H thin films, *J. Appl. Phys.* **120**, 085305 (2016).
- [24] M. Crespin, P. Levitz, and L. Gatineau, Reduced forms of LaNiO_3 perovskite. Part 1.—evidence for new phases: $\text{La}_2\text{Ni}_2\text{O}_5$ and LaNiO_2 , *J. Chem. Soc. Faraday Trans. 2* **79**, 1181 (1983).
- [25] A. Ikeda, T. Manabe, and M. Naito, Comparison of reduction agents in the synthesis of infinite-layer LaNiO_2 films, *Physica C* **506**, 83 (2014).
- [26] M. Hayward, M. Green, M. Rosseinsky, and J. Sloan, Sodium hydride as a powerful reducing agent for topotactic oxide deintercalation: Synthesis and characterization of the nickel (I) oxide LaNiO_2 , *J. Am. Chem. Soc.* **121**, 8843 (1999).
- [27] M. Kawai, S. Inoue, M. Mizumaki, N. Kawamura, N. Ichikawa, and Y. Shimakawa, Reversible changes of epitaxial thin films from perovskite LaNiO_3 to infinite-layer structure LaNiO_2 , *Appl. Phys. Lett.* **94**, 082102 (2009).
- [28] W. Wei, D. Vu, Z. Zhang, F. J. Walker, and C. H. Ahn, Superconducting $\text{Nd}_{1-x}\text{Eu}_x\text{NiO}_2$ thin films using in situ synthesis, *Sci. Adv.* **9**, eadh3327 (2023).
- [29] T. Onozuka, A. Chikamatsu, T. Katayama, T. Fukumura, and T. Hasegawa, Formation of defect-fluorite structured NdNiO_xH_y epitaxial thin films via a soft chemical route from NdNiO_3 precursors, *Dalton Trans.* **45**, 12114 (2016).

- [30] L. Si, W. Xiao, J. Kaufmann, J. M. Tomczak, Y. Lu, Z. Zhong, and K. Held, Topotactic hydrogen in nickelate superconductors and akin infinite-layer oxides ABO_2 , *Phys. Rev. Lett.* **124**, 166402 (2020).
- [31] L. Si, P. Worm, and K. Held, Fingerprints of topotactic hydrogen in nickelate superconductors, *Crystals* **12**, 656 (2022).
- [32] P. Puphal, V. Pomjakushin, R. A. Ortiz, S. Hammoud, M. Isobe, B. Keimer, and M. Hepting, Investigation of hydrogen incorporations in bulk infinite-layer nickelates, *Front. Phys.* **10**, 842578 (2022).
- [33] X. Ding, C. C. Tam, X. Sui, Y. Zhao, M. Xu, J. Choi, H. Leng, J. Zhang, M. Wu, H. Xiao, X. Zu, M. Garcia-Fernandez, S. Agrestini, X. Wu, Q. Wang, P. Gao, S. Li, B. Huang, K.-J. Zhou, and L. Qiao, Critical role of hydrogen for superconductivity in nickelates, *Nature (London)* **615**, 50 (2023).
- [34] S. Zeng, C. S. Tang, Z. Luo, L. E. Chow, Z. S. Lim, S. Prakash, P. Yang, C. Diao, X. Yu, Z. Xing *et al.*, Origin of a Topotactic Reduction Effect for Superconductivity in Infinite-Layer Nickelates, *Phys. Rev. Lett.* **133**, 066503 (2024).
- [35] P. P. Balakrishnan, D. F. Segedin, L. E. Chow, P. Quarterman, S. Muramoto, M. Surendran, R. K. Patel, H. LaBollita, G. A. Pan, and Q. Song, Hydrogen is not necessary for superconductivity in topotactically reduced nickelates, [arXiv:2403.01796](https://arxiv.org/abs/2403.01796).
- [36] G. Bouilly, T. Yajima, T. Terashima, W. Yoshimune, K. Nakano, C. Tassel, Y. Kususe, K. Fujita, K. Tanaka, and T. Yamamoto, Electrical properties of epitaxial thin films of oxyhydrides $\text{ATiO}_{3-x}\text{H}_x$ ($A = \text{Ba}$ and Sr), *Chem. Mater.* **27**, 6354 (2015).
- [37] G. Krieger, A. Raji, L. Schlur, G. Versini, C. Bouillet, M. Lenertz, J. Robert, A. Gloter, N. Viart, and D. Preziosi, Synthesis of infinite-layer nickelates and influence of the capping-layer on magnetotransport, *J. Phys. D: Appl. Phys.* **56**, 024003 (2023).
- [38] C. Lichtensteiger, InteractiveXRDFit: A new tool to simulate and fit x-ray diffractograms of oxide thin films and heterostructures, *J. Appl. Crystallogr.* **51**, 1745 (2018).
- [39] Z. Zhu, V. Shutthanandan, and M. Engelhard, An investigation of hydrogen depth profiling using ToF-SIMS, *Surf. Interface Anal.* **44**, 232 (2012).
- [40] F. Stevie and D. Griffis, Quantification in dynamic sims: Current status and future needs, *Appl. Surf. Sci.* **255**, 1364 (2008).
- [41] S. Fearn, *An Introduction to Time-of-Flight Secondary Ion Mass Spectrometry (ToF-SIMS) and its Application to Materials Science* (Morgan & Claypool Publishers, 2015).
- [42] D. J. Graham and L. J. Gamble, Back to the basics of time-of-flight secondary ion mass spectrometry of bio-related samples. I. Instrumentation and data collection, *Biointerphases* **18**, 021201 (2023).
- [43] C. Magee and E. Botnick, Hydrogen depth profiling using SIMS—problems and their solutions, *J. Vac. Sci. Technol.* **19**, 47 (1981).
- [44] X.-f. Lin, A. Fucsko, K. Noehring, E. Gabriel, A. Regner, S. York, and D. Palsulich, New SIMS method to characterize hydrogen in polysilicon films, *J. Vac. Sci. Technol. B* **40**, 014003 (2022).
- [45] Z. Zhu and V. Shutthanandan, Are cluster ion analysis beams good choices for hydrogen depth profiling using time-of-flight secondary ion mass spectrometry? *Surf. Interface Anal.* **44**, 89 (2012).
- [46] F. Stevie, Analysis of hydrogen in materials with and without high hydrogen mobility, *Surf. Interface Anal.* **48**, 310 (2016).
- [47] A. Marwick and D. Young, Measurements of hydrogen in metal-oxide-semiconductor structures using nuclear reaction profiling, *J. Appl. Phys.* **63**, 2291 (1988).
- [48] H.-B. Li, S. Kobayashi, C. Zhong, M. Namba, Y. Cao, D. Kato, Y. Kotani, Q. Lin, M. Wu, and W.-H. Wang, Dehydration of electrochemically protonated oxide: SrCoO_2 with square spin tubes, *J. Am. Chem. Soc.* **143**, 17517 (2021).
- [49] T. Yajima, A. Kitada, Y. Kobayashi, T. Sakaguchi, G. Bouilly, S. Kasahara, T. Terashima, M. Takano, and H. Kageyama, Epitaxial thin films of $\text{ATiO}_{3-x}\text{H}_x$ ($A = \text{Ba}$ and Sr) ($A = \text{Ba}$, Sr , Ca) with metallic conductivity, *J. Am. Chem. Soc.* **134**, 8782 (2012).
- [50] F. A. Stevie, C. Zhou, M. Hopstaken, M. Saccomanno, Z. Zhang, and A. Turansky, SIMS measurement of hydrogen and deuterium detection limits in silicon: Comparison of different SIMS instrumentation, *J. Vac. Sci. Technol., B: Nanotechnol. Microelectron.: Mater. Process. Meas. Phenom.* **34**, 03H103 (2016).
- [51] P. Kristiansson, M. Borysiuk, L. Ros, H. Skogby, N. Abdel, M. Elfman, E. Nilsson, and J. Pallon, Quantitative hydrogen analysis in minerals based on a semi-empirical approach, *Nucl. Instrum. Methods Phys. Res. Sect. B* **306**, 253 (2013).
- [52] M. Jerigova, V. Szöcs, M. Janek, D. Lorenc, and D. Velic, Muscovite single layer resolution: Secondary ion mass spectrometry depth profile, *Appl. Clay Sci.* **132–133**, 621 (2016).
- [53] S. Hofmann, Sputter depth profiling of thin films, *High Temp. Mater. Processes (London)* **17**, 13 (1998).
- [54] A. Priebe, T. Xie, G. Bürki, L. Pethö, and J. Michler, The matrix effect in TOF-SIMS analysis of two-element inorganic thin films, *J. Anal. At. Spectrom.* **35**, 1156 (2020).